Available online at www.sciencedirect.com
SCIENCE DIRECT®
Applied Radiation and Isotopes 63 (2005) 565–574
Applied Radiation and Isotopes
www.elsevier.com/locate/apradiso

The HYDAD-D antipersonnel landmine detector

F.D. Brooks[a,*], M. Drosg[b]

[a]Department of Physics, University of Cape Town, Rondebosch 7700, South Africa
[b]Institute of Experimental Physics, University of Vienna, A-1090 Wien, Austria

Abstract

HYDAD (HYdrogen Density Anomaly Detection) systems have been developed to detect small (>200 g) antipersonnel landmines (APM) of plastic construction. The HYDAD-D detector is based on the earlier HYDAD designs HYDAD-H and HYDAD-VM. It consists of a neutron source and two identical slow neutron detectors. The difference between the responses of the two detectors is monitored as a function of position in the minefield and APM detection is based on an analysis of this difference. Laboratory tests and Monte Carlo simulations demonstrate that HYDAD-D is capable of detecting the IAEA standard dummy landmine DLM2 at burial depths up to 23 cm in dry sand and at burial depths up to 7 cm in damp sand containing 12% (by mass) water.

Keywords: Landmine detection; Humanitarian demining; Neutron scattering

1. Introduction

HYDAD (HYdrogen Density Anomaly Detection) landmine detectors (Brooks et al., 2004a, b) consist of a source of fast neutrons (AmBe or ^{252}Cf), one or more slow neutron detectors and some electronics for data processing. The neutron detectors sense the increase in slow neutron intensity that occurs when the source–detector are brought in the vicinity of a hydrogen-rich object such as a landmine. The hand-held detector HYDAD-H employs a single slow neutron detector and is manually scanned across the area under investigation at a height of 1–2 cm above the ground surface. The vehicle-mounted detector HYDAD-VM employs an array of six identical slow neutron detectors positioned close to the ground surface. The six detectors are symmetrically dispersed about the fast neutron source which is located 15–25 cm below the surface. Differences between the count rates of the six detectors indicate the presence and approximate location of a landmine. HYDAD-D is a differential type of detector that has evolved from HYDAD-H and HYDAD-VM. It consists of a fast neutron source and two identical slow neutron detectors symmetrically positioned relative to the neutron source. This arrangement detects hydrogen-rich objects by monitoring the difference in count rate between the two slow neutron detectors as the source–detector system is scanned across the object. We present results obtained from laboratory experiments and Monte Carlo simulations that have been undertaken to study the capabilities of this landmine detector and to optimize its design.

2. The HYDAD-D landmine detector

The principle of operation of HYDAD-D may be illustrated by considering a linear scan in which the source–detector system passes over a hydrogen-rich,

*Corresponding author. Tel.: +2721 650 3325; fax: +2721 650 3342.
E-mail address: fbrooks@science.uct.ac.za (F.D. Brooks).

0969-8043/$ - see front matter © 2005 Elsevier Ltd. All rights reserved.
doi:10.1016/j.apradiso.2005.05.006

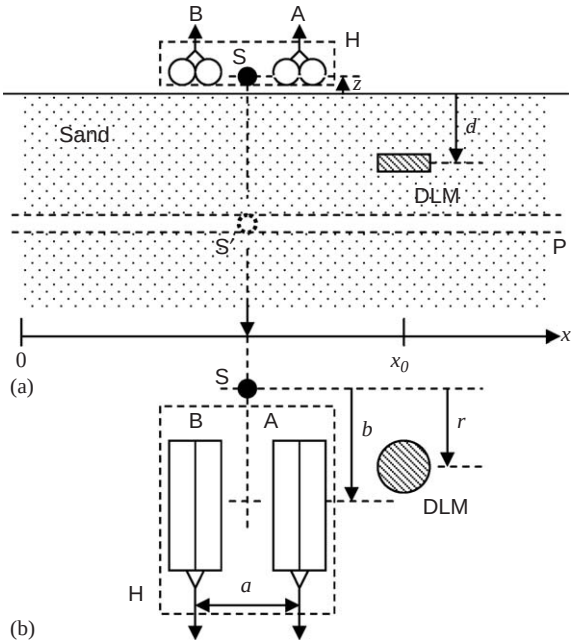

Fig. 1. Schematic diagram of the HYDAD-D test geometry: (a) viewed from the side; and (b) plan view. A and B are the slow neutron detectors of the detector array H. The fast neutron source S is fixed relative to H, either at height $z = 1$ cm above the sand or at S′ ($z = -25$ cm), inside the pipe P which is embedded in the sand. DLM is a dummy landmine or other test object at depth d below the surface of the sand and position $x = x_0$. The lateral displacements of the centres of H and DLM from S are b and r, respectively. H and S move in synchronism in the x-direction.

landmine-like test object DLM as shown in Fig. 1. Taking the source position as the position coordinate x of the system, it can be seen that the count rates of detectors A and B (Fig. 2a) will pass through maxima at different values of x: at $x < x_0$ in the case of detector A and at $x > x_0$ for detector B, where x_0 is the position coordinate of DLM (Fig. 1). Let $A(x)$ and $B(x)$ represent the counts recorded by detectors A and B respectively when S is at position x. The difference count $D(x)$ is given by

$$D(x) = A(x) - B(x). \tag{1}$$

If A and B are identical slow neutron detectors that are insensitive to fast neutrons and the sand containing DLM is homogeneous and dry, then $D(x)$ should vary as shown in Fig. 2b, dropping to zero at points far from $x = x_0$ and describing a positive-then-negative excursion as x increases through and then beyond the value $x = x_0$. Such a positive–negative excursion in $D(x)$ is thus the signature that indicates the presence of a hydrogen-rich object, possibly a landmine. Objects that do not contain significant amounts of hydrogen, for example metal debris, will not imitate this signature and

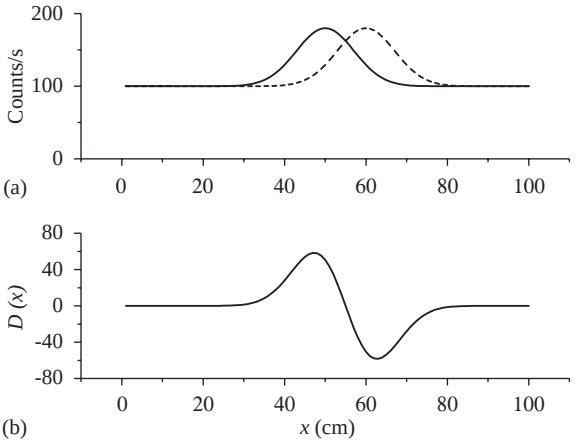

Fig. 2. Schematic illustration of (a) the expected detector count rates $A(x)$ (solid line) and $B(x)$ (dashed line), and (b) the difference count rate $D(x)$, for the example of DLM at $x_0 = 55$ cm.

should therefore not be confused with landmines, as is the case with several other types of landmine detector.

The source–detector geometry of HYDAD-D is similar to that of DUNBLAD, the Delft University Neutron Backscattering Landmine Detector (Datema et al., 2001). However, the data processing and analysis that is used in HYDAD-D to sense the presence of a landmine is different to that employed by DUNBLAD.

3. Test measurements on HYDAD-D

In order to facilitate test measurements the x-coordinate (Fig. 1) was divided into bins n of width 2 cm and counts data were processed as a function of the bin number n instead of the displacement x. Thus Eq. (1) becomes

$$D(n) = A(n) - B(n). \tag{2}$$

The difference $D(n)$ can be expressed in units of the standard deviation σ_D of $D(n)$ by introducing the "separation" $S(n)$ defined as follows:

$$S(n) = D(n)/\sigma_D = D(n)/(A(n) + B(n))^{1/2}. \tag{3}$$

In addition, in order to improve statistical accuracy at the expense of a small reduction in positional accuracy, we introduce an "indicator function" $I(n)$ similar to a "boxcar average" of $S(n)$,

$$I(n) = \sum\nolimits_D / \left(\sum\nolimits_{AB}\right)^{1/2} \tag{4}$$

in which Σ_D and Σ_{AB} are sums of $D(n)$ and of $(A(n) + B(n))$ respectively, taken between the limits of $n_{lo} = n - m$ and $n_{hi} = n + m$, and m is an integer in the range 1–5. A value of $m = 3$ was used for all of the data

presented in this paper. A lower limit of $n_{lo} \geqslant 1$ and an upper limit of $n_{hi} \leqslant N_D$ were imposed, where N_D is the number of bins used in the measurement.

Test measurements were made using a laboratory test bed of dry sand of surface area 80×80 cm and depth 60 cm. The test object for most of the measurements was the IAEA standard dummy landmine DLM2 (Brooks et al., 2004a) that consists of 100 g of TNT-simulant sealed in a cylindrical acrylic container of mass 100 g, diameter 80 mm and height 34 mm. Various other test objects were also studied. Each slow neutron detector (A and B in Fig. 1) consisted of a pair of $^{10}BF_3$-filled proportional counters (type 12EB40, manufactured by Twentieth Century Electronics, UK) connected in parallel. Each proportional counter provided an active volume of 25 mm diam. $\times$ 120 mm, filled to a pressure of 0.5 bar. A cadmium sheet (0.5 mm thick) covered the detector system to shield against thermal neutron background entering from above. Signal outputs from the two detectors were processed by two amplifier-discriminator units and the discriminator outputs were fed via an interface to a desktop computer.

The neutron source S was an AmBe source that emitted $8 \times 10^5\,ns^{-1}$ into 4π. Measurements were made with S either above the sand ($z = 10$ mm), attached to the detector array H, or below the surface ($z = -250$ mm) at position S′ in the pipe P (see Fig. 1). During the latter measurements S and H were coupled together by a string-and-pulley system (not shown in Fig. 1) to ensure that they moved in synchronism with one another, thus maintaining the symmetric geometry between the source and detectors. Test objects were placed at or near the position $x_0 = 25$ cm and buried at different depths d in the sand. Measurements were made with and without single test objects present and for different values of the displacements b and r (see Fig. 1). The distance a between the centres of detectors A and B was 140 mm. A stepping motor drive was used to move the detector system across the test bed at a height of 10 mm above the sand, at constant speed. The scan speed was controlled by the drive frequency applied to the stepping motor, and could be altered by factors of 2 over a range of 8 steps. The dwell times per bin used in the test measurements ranged from 9 to 288 s, with intermediate settings available at 18, 36, 72 and 144 s.

4. Results

Fig. 3 shows results from a measurement made with DLM2 at a depth $d = 24$ mm and displacements $r = b = 0$ mm (Fig. 1). The scan speed used for these measurements provided a dwell time of 72 s per bin. Panel (a) shows the counts per bin measured by detectors A (solid histogram) and B (dashed histogram). Panels (b)–(d) show the quantities $D(n)$, $S(n)$ and $I(n)$ calculated from Eqs. (2), (3) and (4). The calculation of $D(n)$ incorporated a small correction for distortions caused by the finite size of the test bed. The indicator function $I(n)$ (Fig. 3d) obtained from this measurement shows clear "landmine signature" (Fig. 2b). This clear signal can be attributed to the more than adequate dwell time used in these measurements and to the fact that DLM2 was covered by only a few mm of sand and located ($r = b = 0$ mm) so that the source S crossed its diameter during the scan. The signature is less prominent when, for example, d is larger or when a faster scan (shorter dwell time) is used.

In order to obtain a measure of the strength of the observed landmine signature we first compare $I(n)$ with a function of the form shown in Fig. 2b and given by the equation

$$Y(x) = Y_0\{\exp[-(x - x_0 - s)^2/2\sigma^2] - \exp[-(x - x_0 + s)^2/2\sigma^2]\} + Y_B. \quad (5)$$

As in Fig. 2b, $Y(x)$ is expressed as the difference between two Gauss distributions which have the same amplitude Y_0, same standard deviation σ and maxima located at positions x that are displaced from x_0 by $-s$ and $+s$ respectively. The component Y_B is included to allow for the possibility that there may be a small difference between the background rates of detectors A and B. A least squares fit is made to determine a set of "best fit" values for the parameters Y_0, σ, s, x_0 and Y_B, that is the set that minimizes the quantity

$$M = \sum [Y(n) - I(n)]^2/N_D \quad (6)$$

in which the sum is taken over all of the N_D bins used in the measurement and $Y(n)$ is the value of $Y(x)$ calculated at the position x that corresponds to the centre of bin n. The curve in Fig. 3d shows the best fit obtained to the experimental data $I(n)$ (histogram).

Two key features that can be used to identify a landmine signature are: (a) the form of $I(n)$ should match that of Eq. (5), in other words M should be small; and (b) the amplitude Y_0 should be appreciable. In order to obtain a measure of the strength of the landmine signature we therefore introduce a landmine signature parameter P defined by the ratio

$$P = Y_0/M. \quad (7)$$

Thus P will be larger if $I(n)$ is measured with good statistical accuracy, is found to be consistent with the form defined by Eq. (5), and shows a large amplitude Y_0. On the other hand, if the detector scan does not pass close to a landmine or other hydrogen-rich object then the signature component in $I(n)$ will be weak, leading to a low value for Y_0, a larger value for M and hence a low value for P. For the strong signature exhibited by the data shown in Fig. 3d, for example, a value of $P = 29.8$ was obtained. As described below, much smaller values

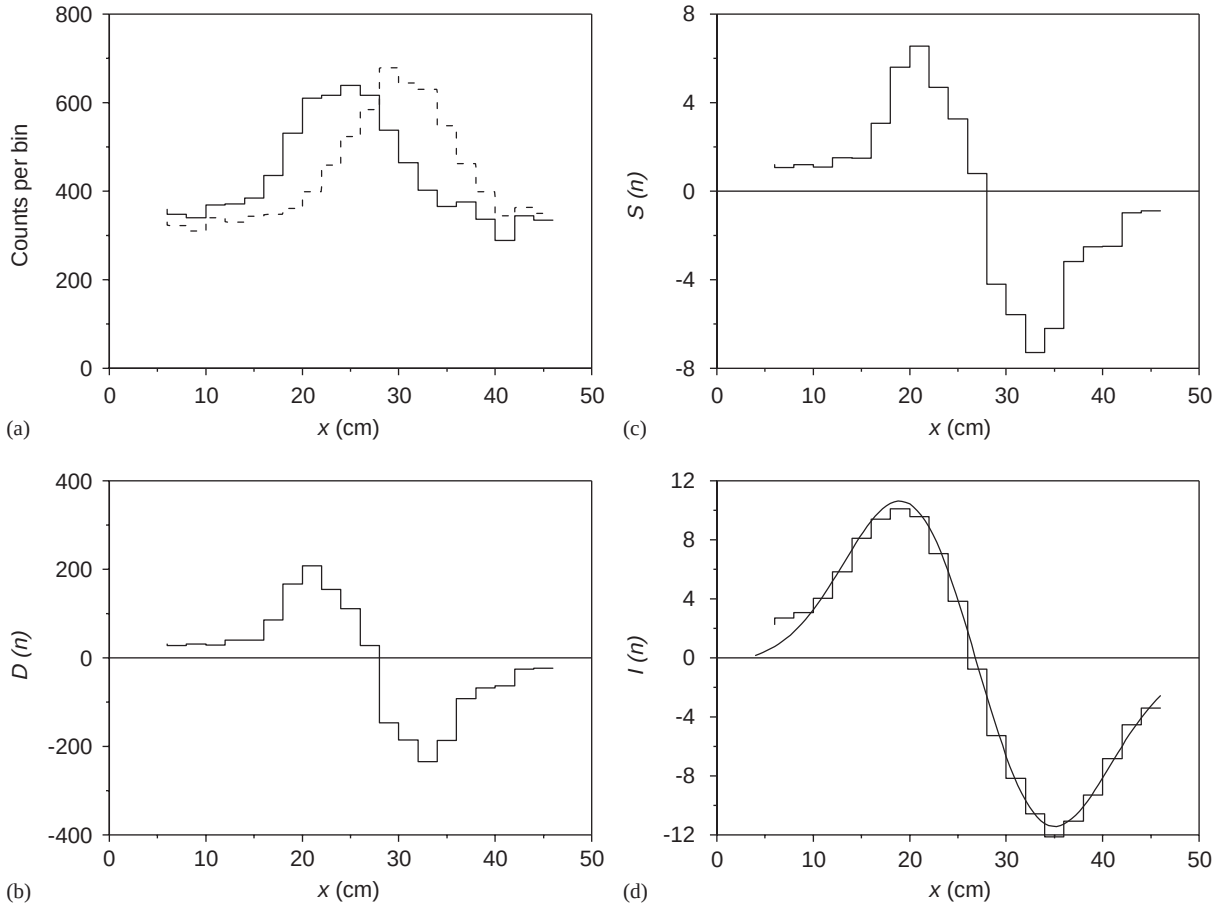

Fig. 3. Data obtained from a scan measurement made using the AmBe neutron source above ground ($z = 10$ mm), test object DLM2 at depth $d = 24$ mm, $r = b = 0$ mm and a dwell time of 72 s per bin: (a) counts per bin from detectors A (solid histogram) and B (dashed histogram); (b) the difference count $D(n)$ (Eq. (2)); (c) the separation $S(n)$ (Eq. (3)); (d) the indicator function $I(n)$ (Eq. (4)) (histogram) and the fit to the landmine signature function $Y(x)$ (Eq. (5)) (curve). The fit led to a value of $P = 29.8$ for the landmine signature parameter (Eq. (7)).

of P are obtained from measurements made using either no test object or test objects that do not contain hydrogen.

Fig. 4 shows experimental results (histograms), least squares fits (curves) and associated values of the parameter P obtained from six further scan measurements made under a variety of conditions. Note in particular that a value of $P = 1.1$ was obtained from the measurement made with no test object (Fig. 4d). Fig. 5 shows values of P obtained from 29 different scan measurements. Before discussing these results further, we present data obtained from Monte Carlo simulations that were undertaken in association with the test experiments. The simulations aimed to provide independent investigations of some of the effects studied in the experiments and also to determine how the landmine detection capability was affected by other factors not studied in the experiments, such as the energy spectrum of the fast neutron source and the presence of moisture in the sand.

5. Monte Carlo simulations

The Monte Carlo code MCNP was used for the simulations. The dummy landmine DLM2 was simulated by a single homogeneous cylinder of the same dimensions, density and average elemental composition as DLM2. The test bed was simulated by a cylinder of quartz sand of density $1.59\,\mathrm{g\,cm^{-3}}$ (when dry), of diameter 90.6 cm and height 60 cm, providing the same sand volume as in the experiments. For convenience in the computation, the neutron source and detectors were stationary relative to the test bed and the source was always located on the cylinder axis. The test object (DLM2) was moved through the sand in order to

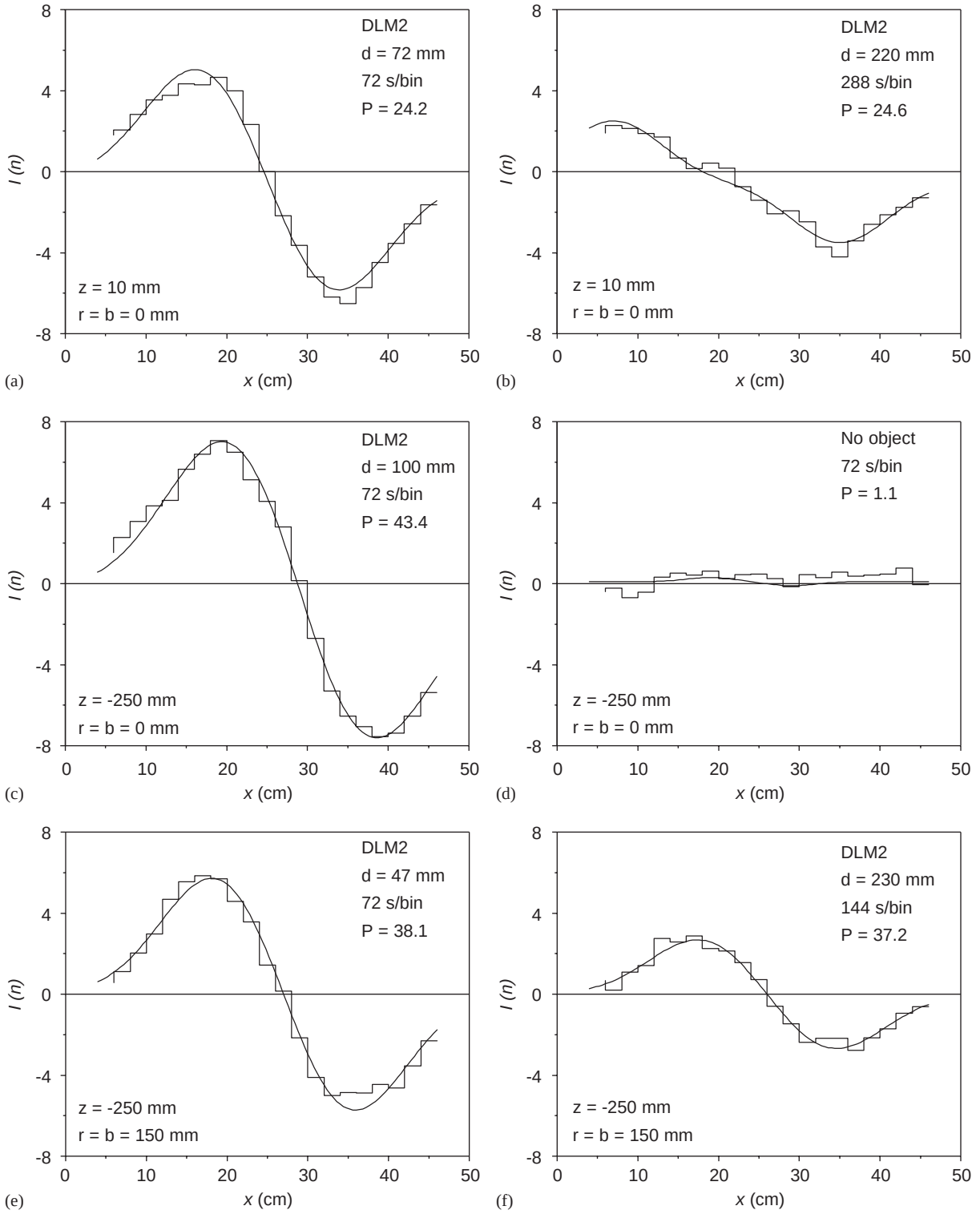

Fig. 4. Experimentally measured indicator functions $I(n)$ (Eq. (4)) (histograms) and fits to the landmine signature function $Y(x)$ of Eq. (5) (curves) obtained using six different combinations of test object, dwell time and values of *d, z, r* and b. Values of the landmine signature parameter P (Eq. (7)) obtained from the fitting are shown in the panels.

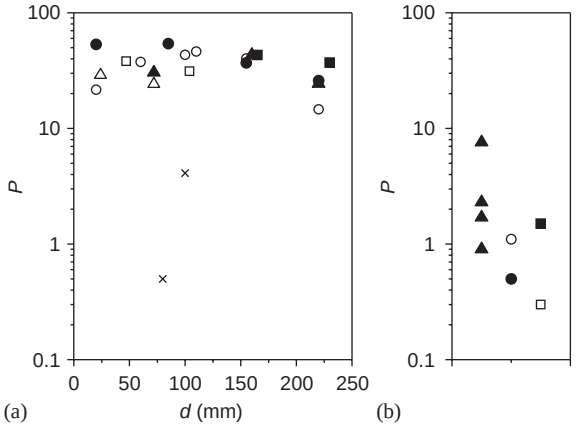

Fig. 5. Values of the landmine signature parameter P (Eq. (7)) obtained by fitting the landmine signature function $Y(x)$ (Eq. (5)) to measurements of the indicator function $I(n)$ (Eq. (4)): (a) P as a function of depth d for measurements made using test object DLM2 (triangles, circles and squares) and other test objects (crosses) (see text); and (b) a display of P-values obtained from measurements made using no test object. Triangles show values from measurements made using $z = 10\,\text{mm}$ and $r = b = 0\,\text{mm}$. Circles and squares show data from measurements made using $z = -250\,\text{mm}$ and $r = b = 0\,\text{mm}$ (circles) or $r = b = 150\,\text{mm}$ (squares). Open symbols indicate that dwell times of 72 s per bin, or less, were used. Solid symbols indicate dwell times of 144 s per bin or longer.

simulate the relative motion between it and the source–detector system. Four different fast neutron sources (labelled 1–4) were simulated: the isotopic neutron sources ^{252}Cf (1) and AmBe (2); and two mono-energetic (accelerator-based) neutron sources dD/2.5 MeV (3) and dT/14.2 MeV (4) that are commercially available as sealed-tube neutron generators. The detector geometry was specified as in Fig. 1. Neutrons entering any proportional counter volume were assumed to be detected by that counter if their energy was less than 10 eV, otherwise not detected. This approximation is not expected to have much influence on the relative accuracy of results that are of interest to us, such as the dependence of count rates on the position of the landmine or on the energy spectrum of the fast neutron source. The counts registered by the four proportional counters in detectors A or B were individually tracked and checked for consistency (allowing for differences in geometry) before summing in pairs to obtain the A and B counts corresponding to the primary measurements made in the experiments (Fig. 3a). The number of neutron histories tracked in each simulation varied between 1 and 5×10^8. All primary results were expressed as detector A and detector B counts per 10^6 neutrons emitted from the source. The difference count $D(n)$ and the separation $S(n)$ were then calculated from Eqs. (2) and (3) respectively.

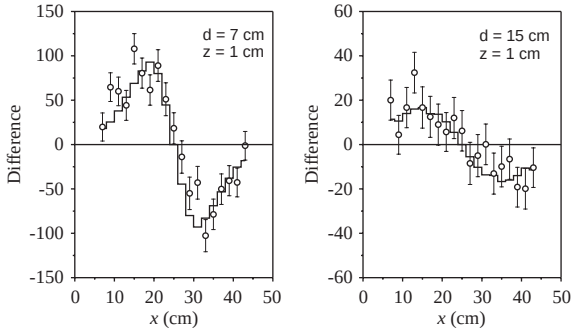

Fig. 6. Difference count $D(n)$ as a function of displacement x obtained from the Monte Carlo simulation (histograms) and from experimental measurements (points). The AmBe source was above ground ($z = 10\,\text{mm}$) and DLM2 was at $x = 25\,\text{cm}$, buried at depths $d = 7\,\text{cm}$ (left panel) and $d = 15\,\text{cm}$ (right panel). The experimental data have been normalized so as to make $\Sigma|D(n)|$ the same as for the simulated data.

Fig. 6 shows plots of $D(n)$ obtained from simulations (histograms) and from experimental measurements (points) made for dry sand, AmBe source at $z = 10\,\text{mm}, r = b = 0\,\text{mm}$ and DLM2 at two different depths, $d = 70$ and $150\,\text{mm}$. The experimental data have been normalized so as to make $\Sigma|D(n)|$ the same as for the corresponding simulated data. These comparisons demonstrate that the simulations reproduce the form of the experimental results perfectly satisfactorily and therefore provide confidence for undertaking further simulations to investigate the performance of HYDAD-D under a variety of conditions.

Fig. 7a shows a comparison of separation values S (Eq. (3)) derived from results simulated for dry sand, $r = b = 0\,mm$ and using the four different neutron sources listed above. For each of the sources, results are shown for four different combinations of the source position z (10 or $-250\,\text{mm}$) and DLM2 depth d (67 or 150 mm). In each case S has been calculated from data simulated at the displacement x that corresponds to the maximum value of the count difference D. This particular value of S corresponds to the maximum value of the counts difference D in "sigma units" and is thus a good measure for comparing the performance of HYDAD-D under different conditions, for example different sources and different values of r, b, z and d. All of the sources give higher S-values at depth $d = 67\,\text{mm}$ (circles) than at $d = 150\,\text{mm}$ (triangles); and for each depth d the S-value obtained with the source underground ($z = -250\,\text{mm}$) (solid points) is higher than that obtained with the source above the surface ($z = 10\,\text{mm}$) (open points). The drop in S on changing from $z = -250$ to 10 mm (solid points to open points) is about twice as large at $d = 150\,\text{mm}$ (triangles) than at $d = 67\,\text{mm}$ (circles). It is particularly interesting to compare the values of S that are obtained from the four neutron

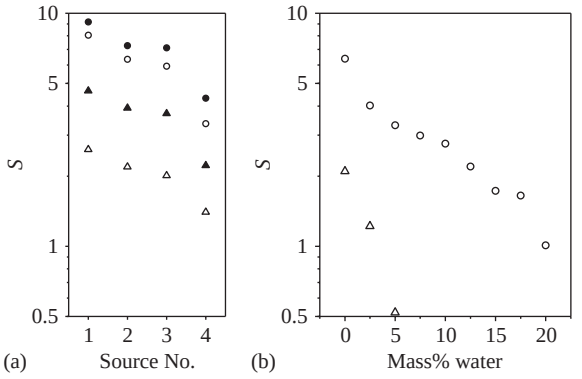

Fig. 7. Plots of the separation S (Eq. (3)) determined from Monte Carlo simulations made using different fast neutron sources, $r = b = 0$ mm, different values of z and d, and different moisture content in the sand. (a) S for different fast neutron sources numbered as follows: (1) ^{252}Cf; (2) AmBe; (3) dD/2.5 MeV; and (4) dT/14.2 MeV.The neutron source was either above ground, at $z = 10$ mm (open points), or below ground, at $z = -250$ mm (solid points). (b) S as a function of the moisture content of the sand, for the AmBe source above ground, at $z = 10$ mm. In both (a) and (b) circles and triangles show data obtained for $d = 67$ mm and 150 mm, respectively.

sources, for the same number of neutrons emitted by the source. The highest S-values are obtained using the ^{252}Cf source. Values obtained using the AmBe source and the dD source are similar to one another and about 20% smaller than for ^{252}Cf . Those obtained using the dT source are more than a factor of 2 smaller than for ^{252}Cf.

Fig. 7b shows the dependence of S on the moisture content (humidity) of the sand. These data were obtained from simulations made using the following input: AmBe source above ground ($z = 10$ mm); $r = b = 0$ mm; $x = 60$ mm; DLM2 at depths $d = 67$ mm (circles) and $d = 150$ mm (triangles). They show that when AmBe is used in the source-above-ground geometry ($z = 10$ mm), HYDAD-D is capable of detecting DLM2 at the "sigma > 2" level ($S > 2$) at depths up to about 70 mm in slightly moist sand (humidity < 12%). They also show that HYDAD-D fails to attain this ($S > 2$) level for detecting DLM2 at depths $d > 150$ mm in sand containing any significant proportion (> 1%) of moisture. Further data are also available from a wide range of simulations of the type represented in Fig. 7, for all of the neutron sources (1–4) and for a range of values of z, d, r, b and soil moisture content.

6. Discussion

Figs. 3–7 provide data that can be used to estimate the potential of HYDAD-D for detecting landmines of size and chemical composition similar to that of the dummy landmine DLM2. From the plots of $I(n)$ shown in Figs. 3d and 4 and the associated values of P it can be seen that detection of such landmines should be feasible at depths d up to 230 mm in dry sand. Furthermore, the measurements made with no test object present, such as Fig. 4d, show that a reliable indication can also be obtained in the absence of any landmine of this type up to a depth of 230 mm. Note that all the data shown in Figs. 3 and 4 except those for $d > 200$ mm (Figs. 4b and 4f) were measured using a dwell time of 72 s per bin. In other words, about 25 min was required to complete the scan across the 21 bins (42 cm) covered in each of these test measurements. The corresponding scan speed of 1.7 cm min^{-1} (1 m h^{-1}) is too slow for practical application to landmine clearing. However, two possibilities for practical operation still appear to be feasible. Firstly, if mine detection to depths beyond 10 cm is not required, reliable operation could be achieved using shorter dwell times and scans could be up to 10 times faster than in the tests, using the same equipment. Secondly, data of the same quality as those obtained in the tests could be obtained more quickly either by using a stronger fast neutron source or by using more efficient slow neutron detectors. Improvements such as these should permit scan speeds 10–20 times faster than those used in the test measurements without sacrifice in the quality of result obtained.

The data shown in Fig. 4b were taken with the neutron source above ground ($z = 10$ mm), using a dwell time of 288 s per bin. The data shown in Fig. 4f were taken with the source below ground ($z = -250$ mm) using a dwell time of 144 s per bin. A comparison of these two measurements made with DLM2 at almost the same depth (220−230 mm) illustrates why there is interest in considering the less convenient geometry in which the neutron source is underground. Longer dwell times were used for these two measurements than for the other measurements shown in Figs. 3 and 4 in order to compensate for the reduced signal-to-background ratio obtained at the greater depth d. Note, however, that a signature of superior quality ($P = 37.2$ compared with 24.6) is obtained with the source below ground (Fig. 4d), even though the dwell time is half that used in the measurement made with the source above ground (Fig. 4b). Thus if the criterion used to identify a landmine signature is that P should exceed a particular value, for example 10, then the minimum measuring time required to detect DLM2 at depths $d > 200$ mm will be less when the neutron source is underground (Fig. 4f) than when it is above ground (Fig. 4b). Results obtained from the Monte Carlo simulations (Fig. 7a) also confirm that more accurate data are obtained with the source below ground than above ground.

Fig. 5a shows a plot of P as a function of d obtained from 21 scan measurements made using DLM2 (triangles, circles and squares) and other test objects (crosses).

Triangles show data from measurements made with the neutron source above ground ($z = 10$ mm). Circles and squares show data from measurements made with the source underground ($z = -250$ mm) and $r = b = 0$ mm (circles) or $r = b = 150$ mm (squares). Open points show data obtained using dwell times of 72 s per bin or shorter. Solid points indicate dwell times of 144 s per bin or longer. The two crosses show data obtained from measurements made using an iron cylinder (4 cm diam. $\times$ 3 cm) at $d = 80$ mm and an empty aluminium soda water can (6 cm diam. $\times$ 7 cm) at $d = 100$ mm. The dwell time was 72 s for these measurements and z, r and b were the same as for the circle points. Fig. 5b shows a display of P-values obtained from 8 measurements made with no test object present in the sand. The ordinate values used in this display are arbitrary and the type of point used indicates the dwell time and the values of z, r and b in the same way as for Fig. 5a.

Fig. 5 shows that the signature parameter P provides an effective criterion for determining whether data obtained from HYDAD-D indicate that a landmine-like object such as DLM2 is present or not. All test measurements made with DLM2 present gave values of $P > 10$. Eight out of ten measurements made without a hydrogenous object present gave values of $P < 3$. Thus provided $I(n)$ is measured with sufficient statistical accuracy (for example, by using a dwell time of at least 72 s per bin under the conditions of the test measurements) these two thresholds can be used to classify measurements into three categories as follows: (a) $P > 10$, a landmine-like object is present (''red''); (b) $P < 3$, no landmine is present (''green''); or (c) $3 < P < 10$, we cannot tell (''amber''). The data in Fig. 5 indicate that a large fraction of the results should fall into the red or green categories. For results that classify as amber, the scan could be extended or repeated to check whether the revised value of P, obtained from a longer measurement, changes the classification to green. If not, then they could be regarded as red. Since the proportion of amber classifications is expected to be small, the additional time required to deal with them in this way should not be excessive.

A comparison of the data measured in the two different geometries studied with the source inside the sand ($z = -250$ mm) can be used to estimate the width of the path that HYDAD-D is capable of scanning in a single sweep. The two geometries in question differ in the lateral displacements of the detector array and test object from the source position, as specified by $r = b = 0$ and 150 mm, respectively (Fig. 1), and are represented by the circles and squares in Fig. 5. From Fig. 5 and also from the data shown in Figs. 4c–f it is seen that good signature measurements can be made at lateral displacements of up to at least 15 cm and probably beyond. This is confirmed by results obtained from the Monte Carlo simulations. From these results we estimate that a path width of about 40 cm, extending 20 cm on both sides of the source, could be covered if four or more pairs of slow neutron detectors were used. Alternatively, a single pair of position-sensitive slow neutron detectors, each of length 40 cm, could be used.

Fig. 8 shows schematic diagrams of two possible arrangements for practical HYDAD-D landmine detector systems. Both arrangements envisage the source–detector being carried on a light trailer or sled which is towed or propelled across the minefield by a mine-protected vehicle. The drive vehicle will be restricted to areas that have already been checked and found to be free of landmines, for example the area immediately behind the detector system or the area alongside its path. The displacement x of the detector system in the direction of the scan will be monitored by an ultrasonic sensor or some other means.

Fig. 8a shows a system based on the source-above-ground geometry. Detectors A and B are commercially available position-sensitive ^{3}He- or $^{10}BF_3$-filled proportional counters. Fig. 8b shows a system based on the alternative geometry employing the fast neutron source underground. The neutron source S is attached to the tip of a rod that is attached to the detector array and projects down into the ground to a depth of about 25 cm. A soil-cutting tool C is mounted in front of the rod. This tool cuts a narrow trench in the sand to allow the rod to move forward freely as the scan advances in the x-direction. The design of the cutter device C might be based on that of a jigsaw, an electrically powered carving knife or a small chain-saw. The detection system incorporates two proportional counters A and B, as in Fig. 8a, together with two or more ''fan detectors'' F which could be conventional ^{3}He- or $^{10}BF_3$-filled proportional counters. The fan detectors monitor the region immediately ahead of the cutting tool to provide early warning of the presence of any landmine in this region and to halt or divert the scan so as to avoid contact with the landmine. The fan detectors will operate in the same way as the HYDAD-VM detector (Brooks et al., 2004a), using the counts provided by detectors A and B as additional references for estimating the ''baseline'' count rate.

The HYDAD-D detector is simple to construct and to operate. All components of the system apart from the detector scanning mechanism are available ''commercially off-the-shelf'' (COTS). The only settings that need to be adjusted when the system is tuned are the pulse height thresholds (or windows) of the two neutron detectors. These are the settings that are used to select low-energy (thermal) neutrons. The fact that landmine detection is based on the difference between the count rates of two identical neutron detectors is a useful feature and a significant improvement over the method used in HYDAD-H (Brooks et al., 2004a). In the absence of a landmine or other hydrogen-rich object the

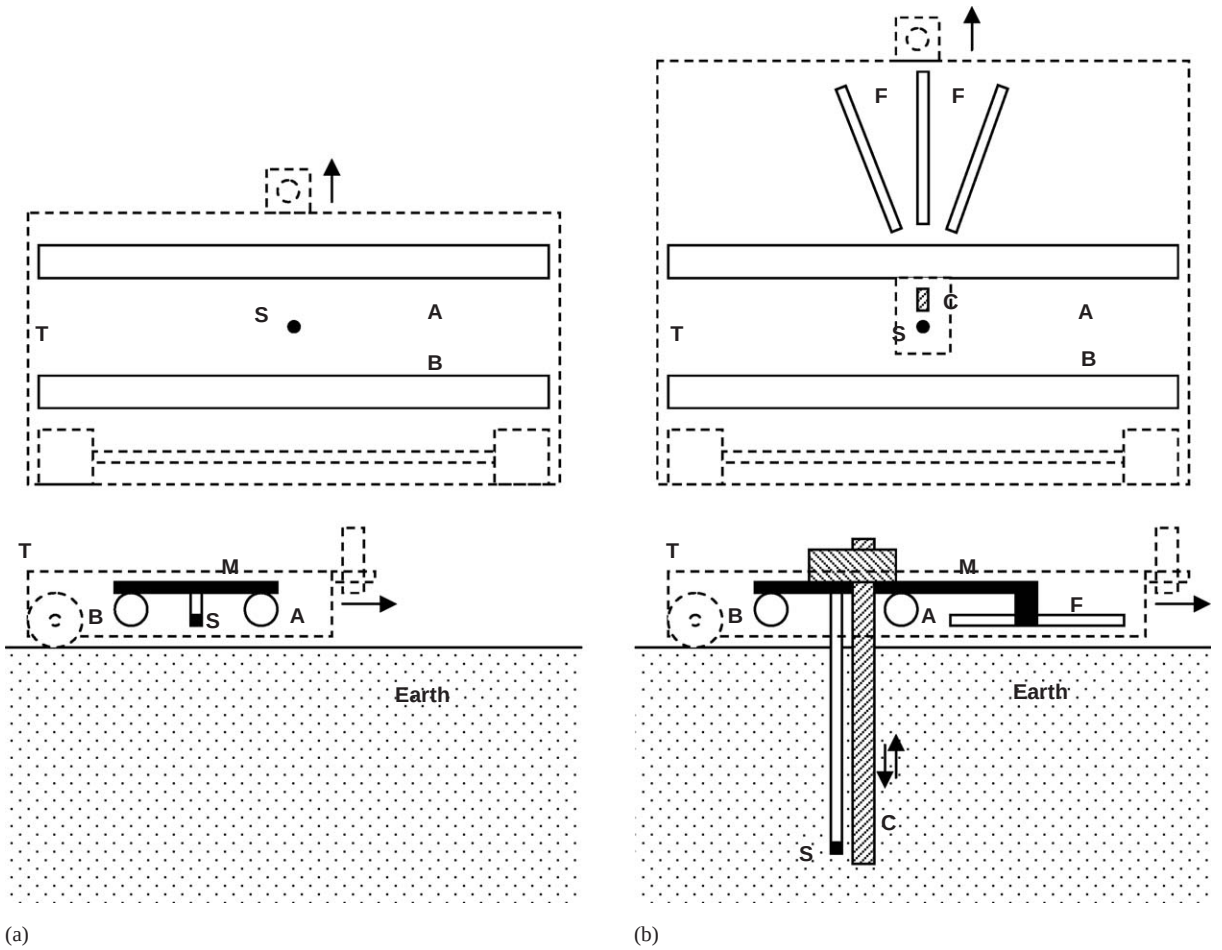

Fig. 8. Schematic diagrams of two proposed geometries for HYDAD-D landmine detectors: (a) a system with the fast neutron source S above ground; and (b) a system with S below ground, advancing along a narrow slit created by the cutting tool C. Plan views are shown above and side views below. Components are: A and B, slow neutron detectors (position-sensitive proportional counters); F, forward-position slow neutron detectors (proportional counters); and M, mechanical framework. The dashed lines T show the outlines of small trailer carts that would be used to carry the detectors across the minefield.

count rates of the two neutron detectors will be the same and will therefore cancel, regardless of what that count rate is. It is only necessary that the sand in the vicinity of the detectors be uniform, particularly in regard to moisture (or hydrogen) content. The tuning of the HYDAD-D detector is therefore insensitive to the hydrogen content of the sand, as long as the hydrogen content is not excessive and does not vary significantly over the dimensions of the detector system. Furthermore, the single count rates of the two neutron detectors also provide an indication of the hydrogen content of the sand, and can thus be used to alert the operator to unexpected variations in the moisture content of the soil.

In summary, the data obtained from these laboratory test experiments and Monte Carlo simulations demonstrate that HYDAD-D has potential for application as a detector of antipersonnel landmines of plastic construction. It should, for example, be suitable for detecting such landmines at depths of up to 23 cm in dry sand, and at depths of up to 7 cm in sand containing 12% (mass) of water. A further series of tests will soon be undertaken in out-of-doors conditions similar to those that apply in real minefields. Monte Carlo simulations will also be undertaken in association with these tests. A hand-held, battery-powered version of HYDAD-D will be tested as well as the two vehicle-driven types illustrated in Fig. 8.

Acknowledgements

We thank the International Atomic Energy Agency for providing financial support and encouragement for this work, through participation in the recent IAEA Coordinated Research Programme on landmine

detection (1999–2003). We also thank Drs. Horst Klein, Helmut Schuhmacher, Volker Dangendorf and Ralf Nolte of PTB, Braunschweig, Germany, for their support and interest, and Andy Buffler, Saalih Allie, Leon van Heerden, Danie Momsen, Dave Boulton and Graham Fowle of the Department of Physics, UCT for their contributions and assistance.

References

Brooks, F.D., Drosg, M., Buffler, A., Allie, M.S., 2004a. Detection of anti-personnel landmines by neutron scattering and attenuation. Applied Radiat. Isot. 61, 27–34.

Brooks, F.D., Buffler, A., Allie, M.S., 2004b. Detection of anti-personnel landmines using neutrons and gamma-rays. Radiat. Phys. Chem. 71, 749–757.

Datema, C.P., Bom, V.R., van Eijk, C.W.E., 2001. Landmine detection with the neutron backscattering method. IEEE Trans. Nucl. Sci. 48 (4), 1087–1091.